Self-Propelled Particles with Soft-Core Interactions: Patterns, Stability, and Collapse

M. R. D'Orsogna,[1] Y. L. Chuang,[1,2] A. L. Bertozzi,[1] and L. S. Chayes[1]
[1]*Department of Mathematics, UCLA, Los Angeles, California 90095, USA*
[2]*Department of Physics, Duke University, Durham, North Carolina 27708, USA*
(Received 15 September 2005; published 17 March 2006)

Understanding collective properties of driven particle systems is significant for naturally occurring aggregates and because the knowledge gained can be used as building blocks for the design of artificial ones. We model self-propelling biological or artificial individuals interacting through pairwise attractive and repulsive forces. For the first time, we are able to predict stability and morphology of organization starting from the shape of the two-body interaction. We present a coherent theory, based on fundamental statistical mechanics, for all possible phases of collective motion.

DOI: 10.1103/PhysRevLett.96.104302 PACS numbers: 45.50.−j, 05.65.+b, 87.23.Cc

The swarming of multiagent systems [1] is a fascinating natural phenomenon. The patterns formed by many self-assembling species pose a wealth of evolutionary [2] and biological [3,4] questions, as well as structural and physical [5–7] ones. In more recent years, understanding the operating principles of natural swarms has also turned into a useful tool for the intelligent design and control of man-made vehicles [8,9].

One of the main unresolved issues arising both in artificially controlled and biological swarms is the ability to predict stability with respect to size. If well defined spacings among individuals exist, swarm size typically increases with particle number, in a ''crystal''-like fashion. This is generally true in animal flocks and might be a desirable feature in robotic systems. On the other hand, natural examples exist of swarms that shrink in size as particle number increases. For instance, in the early development of the *Myxococcus xanthus* or *Stigmatella aurantaca* fruiting bodies two-dimensional bacterial vortices arise and grow until the vortices collapse inward, individual cells occupy the central core, and a localized three-dimensional structure appears [10]. Although many swarming systems have been studied, and specific phase transitions have been observed [4,7,9], a systematic prediction of whether a swarm will collapse or not as the number of constituents increases, has been lacking.

In this Letter, we apply fundamental principles from statistical mechanics to accurately predict the geometry and stability of swarming systems. Specifically, we consider N self-propelled particles powered by biological or mechanical motors that experience a frictional force, leading to a preferred characteristic speed [11]. The particles also interact by means of a two-body generalized Morse potential. Previous related work [5] showed that in some cases localized vortices may form. Here, we explore the *entire* phase space defined by the interaction potential and predict pattern geometry and stability. The identical N particles obey the equations of motion:

$$\frac{\partial \vec{x}_i}{\partial t} = \vec{v}_i, \tag{1}$$

$$m\frac{\partial \vec{v}_i}{\partial t} = (\alpha - \beta|\vec{v}_i|^2)\vec{v}_i - \vec{\nabla}_i U(\vec{x}_i), \tag{2}$$

with the generalized Morse potential given as

$$U(\vec{x}_i) = \sum_{j\neq i}[C_r e^{-|\vec{x}_i-\vec{x}_j|/\ell_r} - C_a e^{-|\vec{x}_i-\vec{x}_j|/\ell_a}]. \tag{3}$$

Here, $1 \leq i \leq N$, ℓ_a and ℓ_r represent the attractive and repulsive potential ranges, and C_a and C_r represent their respective amplitudes. The Morse potential is an example of a pairwise potential: the analysis we present for determining pattern stability can be extended to any type of pairwise interaction, for example, to those in Refs. [7,9], or to power laws. Similarly, the self-propelling term is a driving force choice $f(\vec{v}_i)$ with nontrivial solutions to $f(\vec{v}_i) = 0$.

For velocity independent forces, i.e., $\alpha, \beta = 0$, Eqs. (1)–(3) form a typical Hamiltonian system with conserved energy. The general model belongs to a class of systems—with a root in the dissipation term—that may be approximately mapped onto canonical-dissipative ones, as shown in Ref. [12]. Here, individuals approach configurations for which the total dissipation is zero, so that the dynamics is dictated by the conserved forces. For Eqs. (1)–(3) then, after a transient time $\tau \simeq m/\alpha$, we expect known properties of the conserved case to apply to the general one with $\alpha, \beta \neq 0$. In particular, we expect the conditions for stability of Hamiltonian systems to be applicable. The role of temperature will be played by statistical velocity fluctuations about the asymptotic value $|v_i|^2 = \alpha/\beta$, arising from particle-particle interactions.

For large Hamiltonian systems that obey the laws of statistical mechanics, thermodynamics is expected to emerge as volume and agent number tend to infinity. In order to ensure a smooth passage to the thermodynamic limit, the microscopic interactions must respect certain constraints. The most important of these is *H stability*: for a set of N interacting particles, the total potential energy U is said to be H stable if a constant $B \geq 0$ exists such that $U \geq -NB$ [13]. In particular, this property ensures that particles will not collapse as $N \to \infty$.

Non-H-stable systems are also called catastrophic. Conditions for H stability are explained in detail in Ref. [13]. For example, if the d-dimensional integral of the potential is negative, the system is catastrophic. In this case, as N increases, particles collapse into a dense body with energy per particle proportional to N. On the other hand, for thermodynamic systems, the energy per particle will be asymptotically constant. The stability phase diagram of the Morse potential is shown in Fig. 1, as a function of the ratios $\ell = \ell_r/\ell_a$ and $C = C_r/C_a$.

We numerically integrate Eqs. (1)–(3) using a fourth order Adams-Bashforth method [14], allowing particles an infinite range of motion. Initial conditions are chosen with localized particles of unitary mass and random velocity. The resulting behavior is consistent with the predictions of Fig. 1. Similar techniques can be applied to hard-core power-law potentials where each term in Eq. (3) is divided by $|\vec{x}_i - \vec{x}_j|^p$. For $p \geq 2$ the phase diagram is stable everywhere, but for $p < 2$ a scenario similar to that of Fig. 1 emerges: the separatrix between stable and catastrophic regions is $C\ell^{2-p} = 1$. We focus on the Morse potential and discuss trends for each region of Fig. 1.

In the case $\min\{C, \ell\} < 1$ the potential is catastrophic. For $\beta \neq 0$, particles tend to sustain a constant speed $|\vec{v}_i|^2 \sim \alpha/\beta$, while subject to attractive forces. This competition leads to dynamic configurational patterns. We distinguish three subregions: $\{\ell < C\}$, $\{\ell = C\}$, and $\{\ell > C\}$, respectively, regions I, II, and III of Fig. 1. In region I a potential minimum $d_{\min}$ exists and the N particles self-organize by creating multiparticle clumps. Within each clump the particles travel parallel to each other defining a collective direction. Because of the rotational velocity, this direction changes in time and the clumps rotate about their center of mass [Fig. 2(a)]. Catastrophic behavior is evident in the fact that as N increases, the clumped structures shrink instead of swelling. Interparticle distance also becomes smaller and, eventually, as $N \to \infty$ clumps lose their coherence and merge. The bisectant $\{\ell = C\}$, region II, is the borderline for the existence of extrema. Here, the potential minimum occurs for $d_{\min} = 0$, no associated finite length scale exists, and rings are developed [Fig. 2(c)]. Assuming equidistant particle spacing, the ring radius R may be estimated by balancing the centrifugal and centripetal forces. An approximate implicit expression for R is given by

$$\frac{m\alpha}{2R\beta} = \sum_{n=1}^{N/2} \sin\left(\frac{\pi n}{N}\right) \times \left[\frac{C_a}{\ell_a} e^{-2R/\ell_a \sin[\pi n/N]} - \frac{C_r}{\ell_r} e^{-2R/\ell_r \sin[\pi n/N]}\right]. \quad (4)$$

Estimates of R as given by Eq. (4) match extremely well those obtained numerically as seen in Fig. 2(d). Similar aggregates are also seen Ref. [12]. For $\{\ell > C\}$ in region III of Fig. 1, clumps appear although there is no minimum in the potential. In particular, no intrinsic interparticle spacing exists, and the clumps consist of superimposed particles traveling along a ring: this type of collective motion is energetically more favorable than uniform spacing among particles. An example is shown in Fig. 2(b).

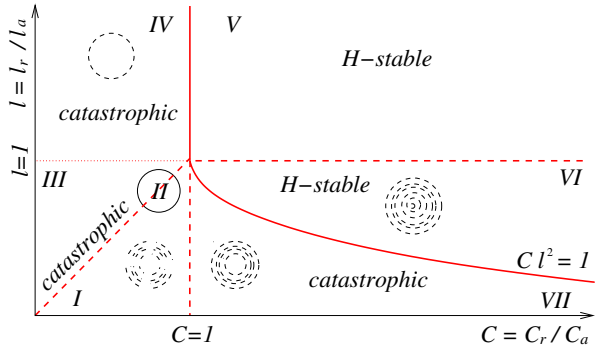

FIG. 1 (color online). H-stability phase diagram of the Morse potential. The catastrophic regions correspond to parameter ratios $\ell = \ell_r/\ell_a$ and $C = C_r/C_a$ for which the thermodynamic limit does not exist. Extrema of the potential d_{ext} exist only for $\ell > \max\{1, C\}$ and for $\ell < \min\{1, C\}$. In these cases $d_{\text{ext}} = \ell_r \log(\ell/C)/(\ell - 1)$. The separatrix is $C\ell^2 = 1$.

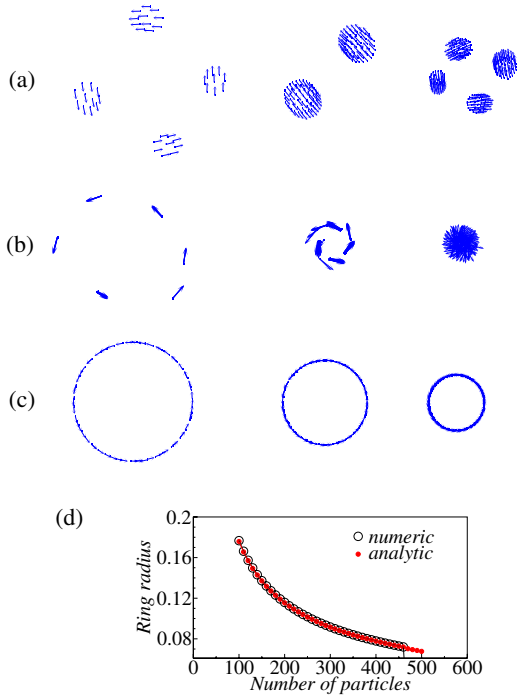

FIG. 2 (color online). Catastrophic geometry. (a) *Clumps*. From left to right $N = 40, 100, 150$. Clumps coalesce as N increases. Parameters are $\alpha = 1$, $\beta = 0.5$, $C_a = \ell_a = 1$, $C_r = 0.6$, $\ell_r = 0.5$. (b) *Ring clumping*. From left to right $N = 40, 100, 200$. Parameters are the same as in (a), but $\ell_r = 1.2$. (c) *Rings*. From left to right $N = 60, 100, 200$. Parameters are the same as in (a), but $C_r = 0.5$. (d) Ring radius as a function of N from numerical data and Eq. (4). Parameters are the same as in (c). The radius scales as $R \sim N^{-0.5}$.

A clumped ring structure also appears in the $\{C < 1 < \ell\}$ regime of region IV. The observed behavior is very similar to what is described in the $\{\ell > C\}$ case above, with the difference that here the potential defines a maximum, and for low particle numbers the extra constraint of avoiding energetically costly interparticle spacings has to be considered. Region V of Fig. 1 where $\max\{\ell, C\} > 1$ corresponds to the H-stable regime. Here, the interparticle potential is characterized by overall repulsive behavior and is minimized by infinite separation. Thus, as $N \to \infty$ the particles will tend to occupy the entire volume at their disposal. The entire region is a "gaseous" phase with particle speed peaked at $|\vec{v}_i|^2 = \alpha/\beta$.

The most interesting region of the phase diagram is defined by $\{\ell < 1 < C\}$, regions VI and VII of the phase diagram. Here, the potential is characterized by short range repulsion and long range attraction. A potential minimum exists and defines a length scale $d_{\min}$. The $C\ell^2 = 1$ curve of Fig. 1 parts the thermodynamically stable region VI from the thermodynamically catastrophic region VII. Although the main features of the two-body potentials are similar, different H-stability properties lead to very different self-organizational behaviors in the moderate and large-particle limits.

Region VI with $\{l/\sqrt{C} < \ell < 1\}$ corresponds to thermodynamic stability. At finite N, and for intermediate α/β, particles approach the characteristic velocity $|v_i^2| = \alpha/\beta$ and reach a kinetic energy much greater than the confining interactions. Agents tend to disperse as individuals. For much smaller of values of α/β, the N particles assemble into organized structures with well defined spacings, which in the large-particle limit tend to a finite value. Particles will then either swarm coherently in a rigid disk aggregate or flock with a finite center of mass velocity, depending on the initial conditions. In both cases, the motion is rigid bodylike and interparticle distances are preserved. For $\alpha/\beta \to 0$, the particles assemble into static, locally crystalline structures.

Region VII where $\{\ell < 1/\sqrt{C} < 1\}$ corresponds to thermodynamic instability; all cases examined in Ref. [5] concern this region. As in the previous case, for finite N, large values of α/β will lead to a gaseous phase and very small values to crystalline structures whose motion is rigid bodylike. However, quite unlike the H-stable scenario discussed above, these are unstable with respect to particle number and in the $N \to \infty$ limit will collapse. At intermediate values of α/β, vortices appear with particles traveling close to the characteristic speed $|\vec{v}_i|^2 \sim \alpha/\beta$. Here, vortex size *decreases* dramatically as a function of particle number as seen in Figs. 3 and 4. Also, for finite N, vortices rotating counterclockwise and clockwise may coexist, depending on the initial conditions. In this regime, the occurrence of double spiraling is visually most dramatic since it occurs within vortices; however, double spiraling is a feature of the entire catastrophic part of the phase

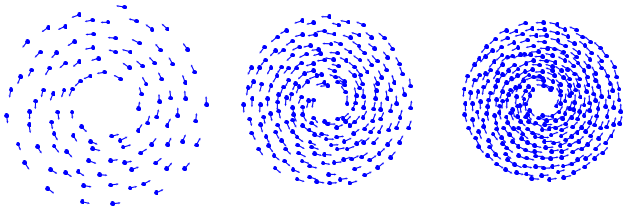

FIG. 3 (color online). Snapshots of swarms for different values of N in the catastrophic regime defined by region VII of Fig. 1. From left to right $N = 100, 200, 300$. The chosen parameters are $C_a = 0.5$, $C_r = 1$, $\ell_a = 2$, $\ell_r = 0.5$, and $\alpha = 1.6$, $\beta = 0.5$.

diagram and occurs in clumped or equispaced rings as well. Double spirals are thus strong indicators of a catastrophic potential. Also, in the catastrophic regime, the total energy is quadratic and energy per particle is linear in N, as seen in Fig. 5. Interparticle separation (not shown) decreases dramatically as $N \to \infty$. For comparison, total energy in the H-stable regime is linear in N while energy per particle and interparticle separation approach constant values.

The swarming behavior of *M. xanthus* cells, which can penetrate each other by crawling, is consistent with catastrophic regime VII of the Morse potential where core-free vortices can arise. These structures are also generated for the power-law interactions previously discussed, with $p < 2$, so that in principle, vortices may be found in other

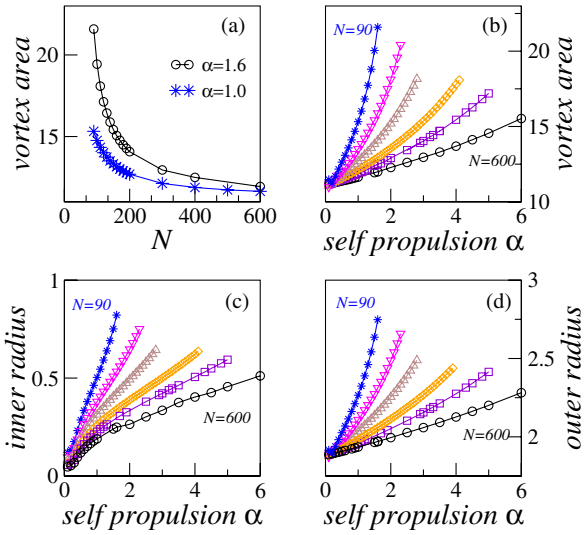

FIG. 4 (color online). Vortex scalings for the catastrophic Morse potential. The parameters are set as in Fig. 3. The friction term $\beta = 0.5$. (a) Vortex area as a function of N for $\alpha = 1.0, 1.6$. Note the dramatic decrease with N. (b) Vortex area as a function of α for various N. From top to bottom $N = 90, 140, 200, 300, 400, 600$. For any fixed α the vortex area decreases with N. (c) Inner and (d) outer radii of the catastrophic vortices as a function of α. The particle numbers are the same as in (b). Both radii increase with α but decrease with N. For large N the inner core disappears.

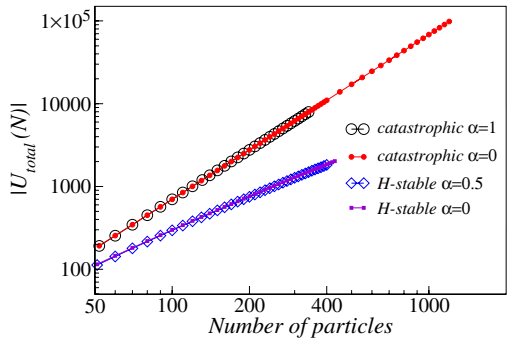

FIG. 5 (color online). Morse potential energy $|U_{\text{total}}| = |\sum_{i=1}^{N} U(\vec{x}_i)|$ as a function of N. Several choices of α are shown with fixed $\beta = 0.5$. The upper curves correspond to the catastrophic regime with the same Morse parameters as in Fig. 3. The scaling law is $|U_{\text{total}}| \sim N^{2.0}$ for both $\alpha = 1$ and $\alpha = 0$. The lower curves correspond to the H-stable parameters $C_a = 0.5$, $C_r = 1$ and $\ell_a = 2$, $\ell_r = 1.5$. The scaling law is $|U_{\text{total}}| \sim N^{1.0}$ for both $\alpha = 0$ and $\alpha = 0.5$. Scaling is linear in the H-stable case, and quadratic in the catastrophic one.

systems that do not allow soft-core interactions. We propose the following qualitative scenario for the initial stages of *M. xanthus* aggregation. As the number of constituents increases, so does particle speed $\sqrt{\alpha/\beta}$. This is consistent with the observed enhancement of C-signal activity among particles [15] that increases motility. The bacterial vortex then increases its size with N and double spirals may coexist, as reported in the literature [16]. Eventually, bacterial speed reaches an upper limit and increasing N leads to vortex collapsed behavior, until, finally, a complex 3D structure evolves [17] due to finite height of the cells and other features not accounted for in Eqs. (1)–(3).

The methodology we present is valid for any type of interaction, not only soft-core ones. The Morse potential is a rich, illustrative example with catastrophic and stable phases. In spite of its name, a catastrophic regime might add versatility to the development of unmanned vehicular technology. Vehicles could be programmed to cross over from H-stable to catastrophic behaviors, shifting from a dispersive (searching) mode to convergence at a specific site. Finite hard cores superimposed on catastrophic potentials are felt only when interparticle separations are comparable to the hard-core radius. Structures then coalesce catastrophically until the number of constituents reaches a cutoff N^*. Finally, our model is deterministic: a more realistic description would include the presence of noise. Preliminary results show that moderate noise levels do not dramatically affect the patterns seen here. Larger fluctuations lead to ruptures or morphological changes.

We thank H. Levine, D. Marthaler, and T. Chou for useful discussions. We acknowledge support from NSF, ARO, and ONR through Grants No. DMS-0306167, No. W911NF-05-1-0112, and No. N000140610059.

[1] S. Camazine *et al.*, *Self Organization in Biological Systems* (Princeton University Press, Princeton, 2003); I. Prigogine, *Order Out of Chaos* (Bantam, New York, 1984).

[2] J. K. Parrish and L. Edelstein-Keshet, Science **284**, 99 (1999); S. A. Kaufmann, *The Origins of Order: Self-Organization and Selection in Evolution* (Oxford University Press, New York, 1993).

[3] I. D. Couzin, J. Krauss, N. R. Franks, and S. A. Levin, Nature (London) **433**, 513 (2005); I. Riedel, K. Kruse, and J. Howard, Science **309**, 300 (2005); G. Flierl, D. Grünbaum, S. A. Levin, and D. Olson, J. Theor. Biol. **196**, 397 (1999).

[4] I. D. Couzin, J. Krause, R. James, G. D. Ruxton, and N. R. Franks, J. Theor. Biol. **218**, 1 (2002).

[5] H. Levine, W. J. Rappel, and I. Cohen, Phys. Rev. E **63**, 017101 (2001).

[6] J. Toner and Y. Tu, Phys. Rev. Lett. **75**, 4326 (1995); T. Vicsek *et al.*, Phys. Rev. Lett. **75**, 1226 (1995); N. Shimoyama *et al.*, Phys. Rev. Lett. **76**, 3870 (1996); E. V. Albano, Phys. Rev. Lett. **77**, 2129 (1996); G. Grégoire and H. Chaté, Phys. Rev. Lett. **92**, 025702 (2004).

[7] A. Mogilner, L. Edelstein-Keshet, L. Bent, and A. Spiros, J. Math. Biol. **47**, 353 (2003).

[8] E. Bonabeau, M. Dorigo, and G. Theraulaz, *Swarm Intelligence: From Natural to Artificial Systems* (Oxford University Press, New York, 1999); N. E. Leonard and E. Fiorelli, in *Proceedings of the 40th IEEE Conference on Decision and Control* (IEEE, Piscataway, NJ, 2001), p. 2968; E. W. Justh and P. S. Krishnaprasad, in *Proceedings of the 42nd IEEE Conference on Decision and Control* (IEEE, Piscataway, NJ, 2003), p. 3609.

[9] V. Gazi and K. Passino, IEEE Trans. Autom. Control **48**, 692 (2003).

[10] A. L. Koch and D. White, Bioessays **20**, 1030 (1998); S. Kim and D. Kaiser, Science **249**, 926 (1990).

[11] R. Hilborn, *Chaos and Nonlinear Dynamics* (Oxford University Press, New York, 2001).

[12] F. Schweitzer, W. Ebeling, and B. Tilch, Phys. Rev. E **64**, 021110 (2001); U. Erdmann, W. Ebeling, and V. Anishchenko, Phys. Rev. E **65**, 061106 (2002).

[13] D. Ruelle, *Statistical Mechanics, Rigorous Results* (W. A. Benjamin, Inc., New York, 1969).

[14] G. H. Golub and James M. Ortega, *Scientific Computing and Differential Equations: An Introduction to Numerical Methods* (Academic Press, New York, 1992).

[15] L. Jelsbak and L. Sgaard-Andresen, Proc. Natl. Acad. Sci. U.S.A. **99**, 2032 (2002).

[16] O. A. Igoshin, R. Welch, D. Kaiser, and G. Oster, Proc. Natl. Acad. Sci. U.S.A. **101**, 4256 (2004); K. A. O'Connor and D. R. Zusman, J. Bacteriol. **171**, 6013 (1989).

[17] J. M. Kuner and D. Kaiser, J. Bacteriol. **151**, 458 (1982); D. Kaiser, Nat. Rev. Microbiol. **1**, 45 (2003).